



# Improvement of fluidization quality of a LiF bed using internal blades

Chunbo Hu, Pingyu Zhang, Xinlong Wang, Xiushan Yang, Lin Yang, Zhiye Zhang, Xingjian Kong\*

School of chemical engineering, Sichuan University, 610065 Chengdu, China

## ARTICLE INFO

### Article history:

Received 26 March 2019

Received in revised form 4 November 2019

Accepted 6 December 2019

Available online 9 December 2019

### Keywords:

Internal blade

Fluidization ability

LiF

Agglomerate mechanism

## ABSTRACT

This reported investigation dealt with the effect of the addition of internal blades to a fluidized bed and how this modification affected the bed's minimum fluidization velocity and the particle agglomerate size of LiF. This modification resulted in a new concept of dimensionless fluidization that can be used to quickly compare the fluidization quality of various types of fluidized beds. The experimental results showed that the fluidization in the bed that contained internal blades was better than the fluidization of a bed containing only LiF powder. When internal blades were added, large aggregates were found to collide with the blades and the walls of the bed as a result of airflow, resulting in fragmentation and improved fluidization of smaller aggregates. A vertical component force of the internal blades was used to modify the original Zhou-Li force balance model. The calculated results for the agglomerates in the LiF internal blade-bed using the modified Zhou-Li equation agreed well with the experimental data. Therefore, it was concluded that the modified Zhou-Li equation was adequate for predicting the size of the LiF agglomerates in a fluidized bed.

© 2019 Elsevier B.V. All rights reserved.

## 1. Introduction

LiPF<sub>6</sub> is an important supporting salt in the electrolyte in Li-ion batteries [1], and electrolytes containing this supporting salt meet the basic requirements for the electrical conductivity and chemical stability in lithium ion batteries. The preparation of LiPF<sub>6</sub> using the gas-solid method [2] is relatively easy to accomplish. The gas-solid fluidized bed reactor provides increased heat and mass transfer efficiency [3] between the two reaction phases, because the C-type viscous LiF particles exhibit non-ideal fluidization. However, new methods to improve the fluidization quality of the LiF particles have become an important issue.

The main feature of Class C materials is that they exhibit good viscosity, but it is difficult for these materials to form a normal fluidized state, because they are subject to slugging and channel flow [4,5]. The root cause of this problem is that the viscous force between the particles is greater than the drag imparted by the fluid. Particle size is generally the culprit in the generation of viscous forces, coupled with strong electrostatic forces, and large quantities of moisture [6–8]. According to Liu [9], ultra-fine particles have very large viscous forces. At a certain critical velocity, a number of small agglomerates is formed for fluidization, so that a Gaussian distribution occurs in the size of these agglomerates. LaMarche et al. [10] concluded that the cohesive force of the viscous particles was very sensitive to the particle surface roughness, so that the fluidization process of a fine powder could be divided into three stages, which are the elastic particle stage, the conversion stage, and the agglomeration fluidization stage.

Fluidization modification of C-type particles can usually be accomplished by one of two methods [11]; however, the internal method is plagued by the separation of added components. Therefore, to improve the fluidization of the cohesive particles, an external force field is usually employed to weaken and overcome the cohesion between the cohesive particles and reduce the size of the agglomerates. Cano et al. [12] investigated the fluidization of ultrafine particles in a vibrating field, and found that high frequency vibration decreased the minimum fluidization velocity, and a higher vibration amplitude reduced the bubble velocity. Guo et al. [13] found that the fluidization quality of nanoparticles was significantly increased by an increase in the level of sound pressure (100–103.4 dB). Jiang et al. [14] installed four annular baffles with 56% porosity in a circulating fluidized bed to improve the ozone decomposition of FCC catalysts. Jing's results showed that the baffles enhanced the radial mixing of the particles and gases, which improved the gas-solid contact efficiency. Liu et al. [15] reported a study of the improvement of internal components in the fluidization of viscous particles, and their experiments showed that inclusion of pore-paddles provided the best improvement in the fluidization, which was a better approach than increasing the number of blades in the bed. They also found that achieving a satisfactory effect required that the slant angle of the blades should be >60°, and the opening rate of blades should be 25%. In addition to the prediction and estimation of the size of viscous particles, Antonio et al. [16] proposed a simple equation to estimate the size of the aggregates obtained when fluidization equilibrium is obtained. That is to say, attainment of a balance between the local shear force on the outer particles and the interparticle adhesion. Chaouki et al. [17] estimated the size of a particle cluster by assuming that the difference between the gravitation force acting on the cluster

\* Corresponding author.

E-mail address: [kongxingjian@scu.edu.cn](mailto:kongxingjian@scu.edu.cn) (X. Kong).

### Nomenclature

$U_{mf}$  minimum fluidization velocity, m/s.  
 $U$  superficial gas velocity, m/s.  
 $P$  pressure drop cross the fluidized bed, Pa.  
 $F_y$  drag force, N.  
 $F_g$  apparent gravity, N.  
 $F_{va}$  Van der Waals force, N.  
 $F_c$  collision force, N.  
 $F_N$  vertical component force.  
 $da$  agglomerate size,  $\mu m$ .  
 $Hr$  relative height.  
 $f_a$  fluidization ability.  
 $w$  mass percentage, %.  
 $H_a$  Hamaker constant, dimensionless.  
 $B$  Boltzmann constant, J/K.  
 $T$  absolute temperature, K.  
 $h$  Planck constant, J·s.  
 $n_0$  refractive index, dimensionless.  
 $V$  relative collision velocity, m/s.

### Greek symbols

$\varepsilon$  bed voidage, dimensionless.  
 $\delta$  distance between two departing particles, m.  
 $\nu_e$  ultraviolet adsorption frequency,  $s^{-1}$ .  
 $\varepsilon_0$  dielectric constants, dimensionless.  
 $n_0$  refractive index, dimensionless.  
 $\rho_a$  average density of the agglomerates ( $kg/m^3$ ).

and its buoyancy was equal to the van der Waals forces at a single point of contact of the particles. Morooka et al. [18] estimated the size of the agglomerates by using the principle of energy balance. Gidaspow [19] described the collision dynamics of two particles, and the Zhou-Li [20,21] equation allows for an iterative calculation of the size of the agglomerates in the case of purely viscous particles.

However, all of these studies ignored the estimated size of the fluidized agglomerates after the addition of internal fittings that a fluidized bed. Based on these reported literature studies, this currently reported effort focused on improvements to the fluidization of LiF particles that was provided by internal mixing blades. In addition, the Zhou-Li equation was modified to assist in describing the mechanism of the

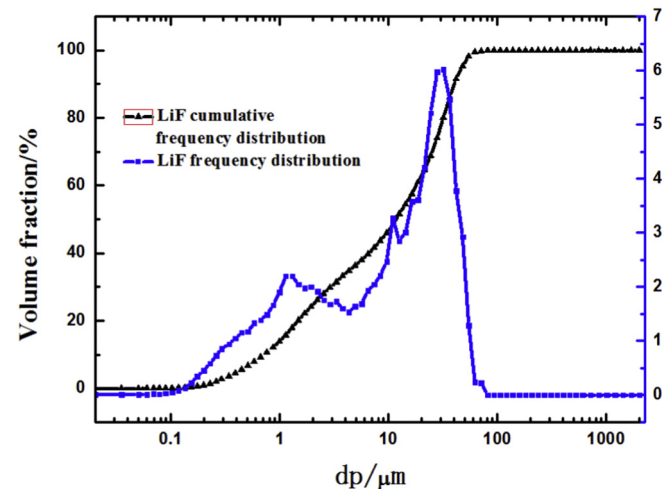


Fig. 1. The curve of LiF particle-size distribution.

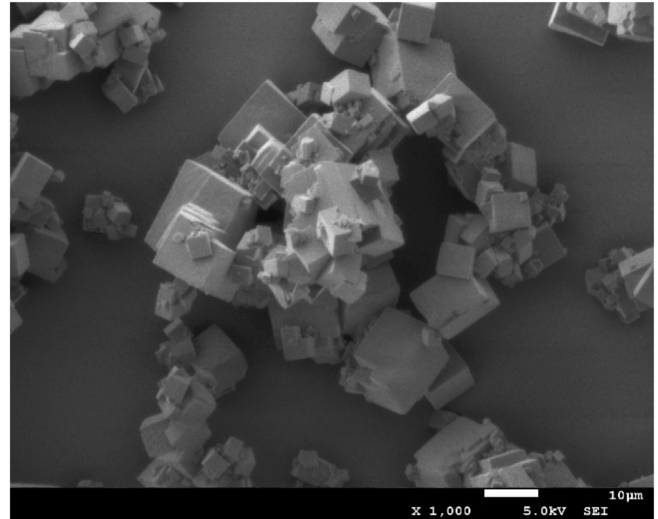


Fig. 2. The SEM image of LiF particles.

improvement provided by the internal blades to the fluidization of class C viscous particles.

## 2. Experimental

### 2.1. Particles, internals and pressure acquisition

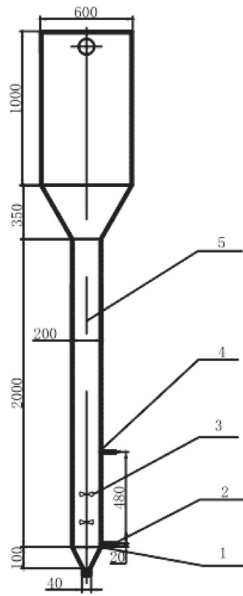
The average particle diameter of LiF used in the reported experiments was  $16.645 \mu m$ , the bulk density was  $0.76 g/cm^3$ , and the compaction density of the material was  $1.16 g/cm^3$ . When in the state of natural accumulation, multiple particles spontaneously accumulate to form an aggregate.

The diameter of the internal blades was 160 mm, and their thickness was 0.5 mm. Two, three and four blades were used in the experimental apparatus and the torsion angle of these blades was varied between  $50^\circ$ ,  $55^\circ$ ,  $60^\circ$  and  $65^\circ$ . The experimental fluidized bed was a 2.5 dimension, half-section bed, and the blade was an internal half-blade. Fig. 3 shows the internal blade design for 3 blades at  $55^\circ$ , and Fig. 4 shows the actual installation. (See Figs. 1 and 2.)

A CY200 digital pressure sensor obtained from the Chengdu Testing Company was used in these experiments, as shown in Fig. 5. The CY200 series digital pressure sensor uses a SOC (single chip system) chip, a piezoresistive silicon crystal and microprocessor for data processing and storage for filtering, amplification, A/D conversion and correction of the pressure signal data.



Fig. 3. Blade internal. 1. distrvtion plate 2. lower pressure sensor 3. blade internal 4. upper pressure sensor 5. fluidized bed.



1. distribution plate
2. lower pressure sensor
3. blade internal
4. upper pressure sensor
5. fluidized bed

Fig. 4. Installation of blade internal.



Fig. 5. The pressure sensor.

### 2.2. Experimental apparatus and method of evaluation

A schematic flow diagram of the experimental, pilot fluidized bed used in this study is shown in Fig. 6 and the specifications of the fluidized bed and the range of operating variables are listed in Table 1. The

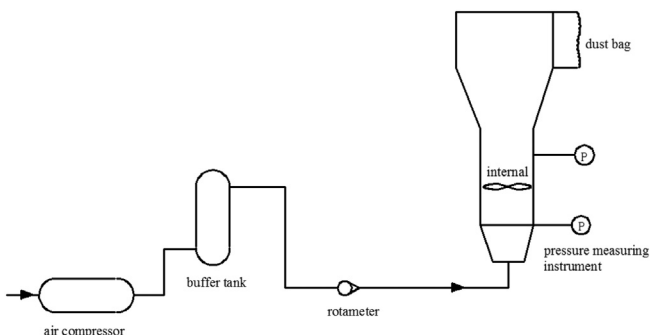


Fig. 6. Schematic illustration of the fluidized bed.

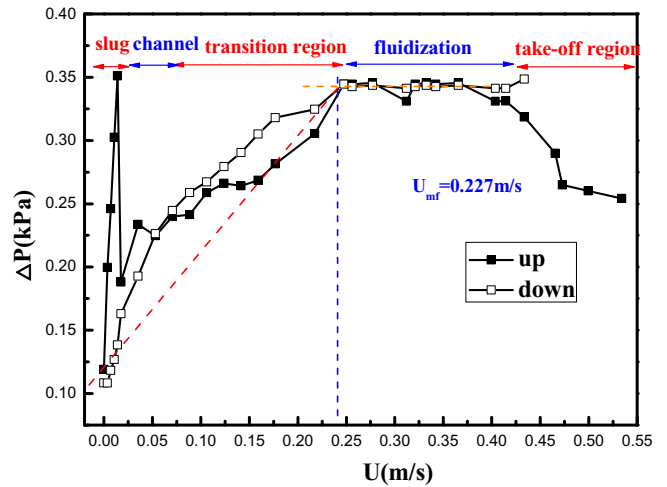


Fig. 7. Fluidized pressure fall-off curve of LiF powders at 3 kg.

fluidized bed was fabricated from a cylindrical glass tube to enable easy observation of the fluidization behavior of the particulate bed.

After being dried in an oven for 2 h at about 120 °C, the LiF powder was loaded into the fluidized bed, and air was fed into the bottom of the column using an air compressor. Flow meters were used to supply and control the flow rate of gas, and CY200 pressure sensors were used to measure the fluidization parameters. The bed height of the particles was fixed at about 23 cm before the experiments were initiated. In addition, after each experiment reached the initial fluidization state and remained stable for 2 min, sampling of the particle cluster was conducted at the side of the bed body 20 cm above the distribution plate. Cluster samples were taken from the bed each minute during the test for five minutes and the sampled material was examined under a microscope. The average particle cluster size value was calculated as the measured value of the cluster size after adding the internal blades to the bed.

In addition to the traditional methods used evaluate the fluidization quality of LiF particle bed, including the lifting pressure drop curve and bed expansion, this study proposed a new concept termed dimensionless fluidization, which is defined as:

fluidization ability

$$= \frac{\text{expansion ratio}}{\text{minimum fluidization velocity/particle take-off speed}} \quad (1)$$

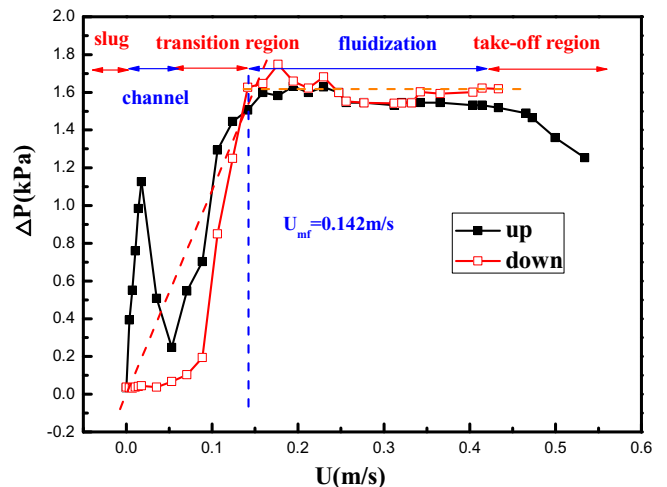


Fig. 8. Fluidized pressure fall-off curve of LiF powders with blade internal.

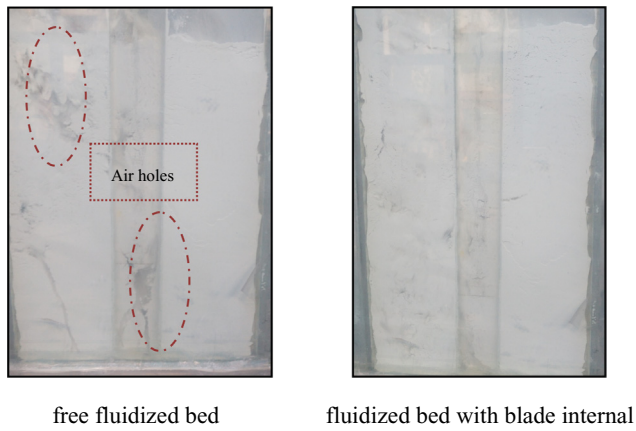


Fig. 9. LiF powders fluidized photos at the speed of 0.142 m/s.

This dimensionless fluidization capability (abbreviation for  $f_a$ ) can be used to quickly compare the relative quality of fluidization of various types of fluidized beds. The particle take-off speed is inherent to the system and is related to its physical properties. Therefore, the numerator in this relationship is related only to the minimum fluidization velocity. Consequently, the smaller the minimum fluidization velocity, the larger the adjustable space in the process. The value of the numerator is the relative expansion ratio of the bed at the minimum fluidization velocity of a dense phase bed system, which is directly related to the bed void ratio. Therefore, a good state of fluidization in the bed will produce a larger  $f_a$  value. Under fixed conditions, a high dimensionless fluidization of the bed will produce better fluidization quality in the system.

### 3. Results and discussion

#### 3.1. Comparison between free bed and internal bed

Fig. 7 and Fig. 8 represent the pressure drop curves of the LiF fine particles fluidized in a free bed and an internal bed. As can be seen from Fig. 7, when an internal blade is absent, the drop in the bed pressure increases rapidly as the gas velocity increases and the powder remains in a plunger state due to the viscosity of the particle bed. As the gas velocity continues to increase, the pressure drop in the bed rapidly decreases and remains low due to the presence of huge holes in the particle bed and air holes inside the bed, so that the gas short-circuits the

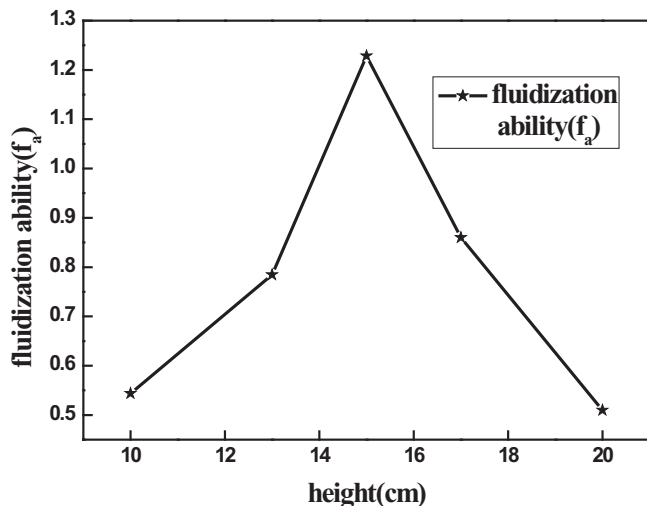


Fig. 10. Fluidization ability curve of LiF with different installation height of blade internal.

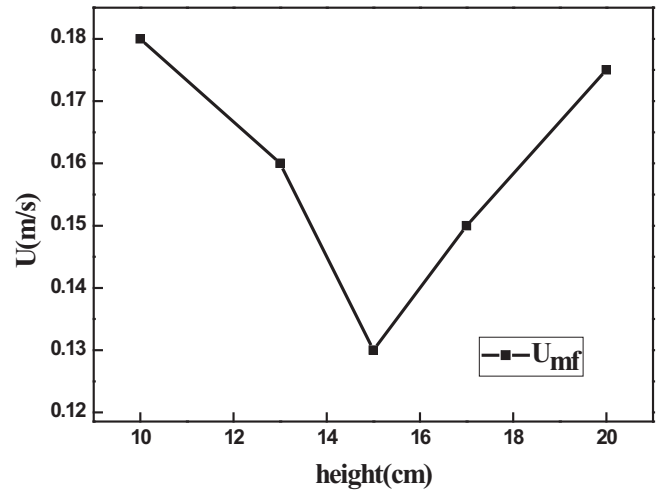


Fig. 11. The minimum fluidization velocity curves of LiF with different installation height of blade internal.

entire bed and forms flow channels. A continuing increase in the air inlet velocity causes the bed to collapse and fluidize, so that the bed is in a transition stage of partial fluidization. As shown in Fig. 8, with the addition of an internal blade, there is a larger pressure drop across a layer of the bed at the same gas velocity as when the bed layer has no blade, and the obstruction caused by the blade is one of the reasons for this increase in pressure drop. In addition, under the same gas velocity conditions, the addition of internal blades improves the fluidization of the whole bed, and the partial fluidization stage of the fluidized bed is obviously less than that of the free bed, the channel flow area is reduced, and the bed pressure drop is increased. At the same time, the addition of internal blades also disrupts the agglomeration of the viscous LiF particles. The experimental photos are shown in Fig. 9 and data are listed in the attached table.

free fluidized bed fluidized bed with blade internal.

#### 3.2. Effect of mounting height of internal blades on bed fluidization

Fig. 10 shows fluidization curves that are produced by mounting the blades at various heights in the bed. It can be clearly seen from the results shown in this figure that an increase in the height of the blade resulted in increased bed fluidization that could be expressed as a quadratic function. There was a maximum

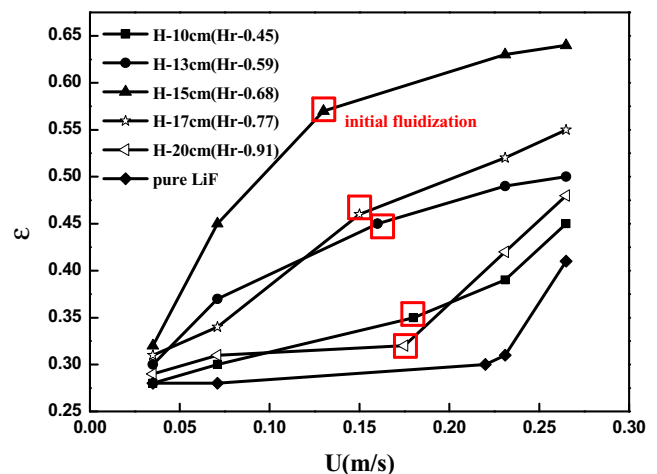


Fig. 12. Expansion rate curve of LiF with different installation height of blade internal.

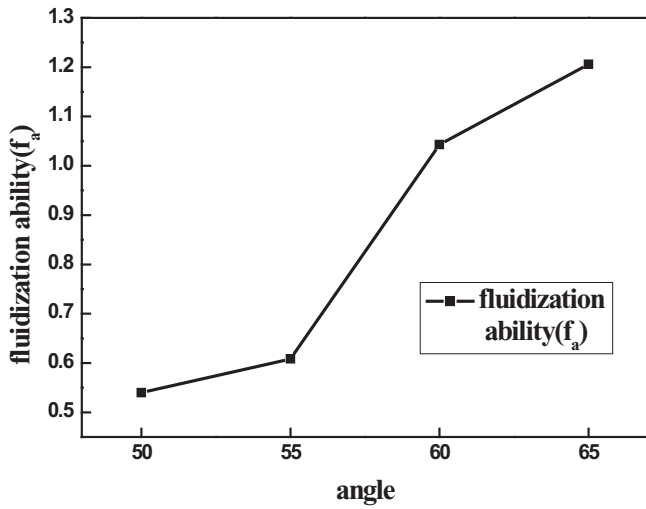


Fig. 13. Fluidization ability curve of LiF with different angle of blade internal.

value of fluidization at an installation height of 15 cm (the relative height  $H_r$  is the ratio of the absolute installation height to the static bed height), so that the LiF particle fluidization was best at this blade installation height. Channel flow easily occurs in the fluidization of C particles, because of uneven pressure drops in the bed and the easy agglomeration of these particles. When the height of installation was too low (10 cm), the effective area of the internal blades was too small, which precluded the crushing of the cluster and the redistribution of pressure drop across the distribution plate. When the installation height exceeded the optimum installation value, the channel flow was stable, and the effect of the internal blade on the redistribution of pressure drop at the distribution plate was significantly reduced. Consequently, it was concluded that the internal component did not disrupt the channel flow to cause either breakage of the particle agglomerates or produce clustering. Therefore, 15 cm was chosen as the optimum installation height for internal blades in the 3 kg LiF fluidization bed experiments. In the following sections, the internal blades were all installed at 15 cm in the test beds. The fluidization capacity was consistent with the minimum fluidization velocity (Fig. 11) and the bed expansion rate (Fig. 12), so the

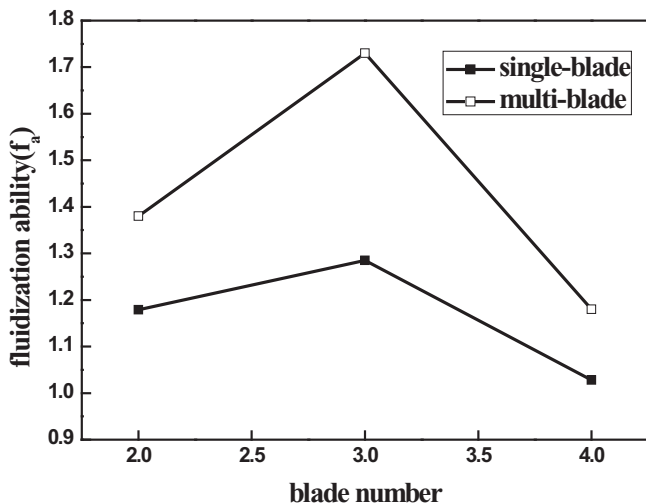


Fig. 14. Fluidization ability curve of LiF with different blade internal.

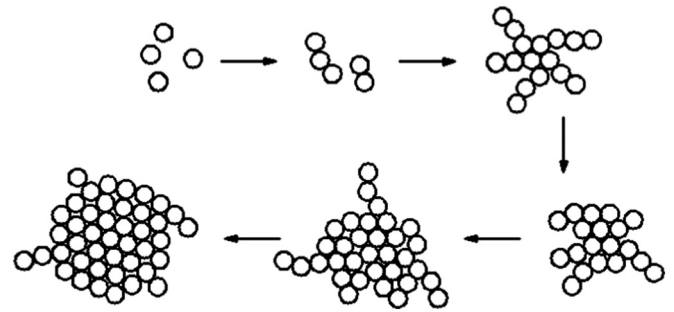


Fig. 15. Mechanism of particle agglomeration.

dimensionless fluidization ability,  $f_a$  was used to evaluate fluidization quality in the various systems.

### 3.3. Effect of the torsion angle of the internal blade on bed fluidization

Fig. 13 shows the effect of the torsion angle of internal blades on the bed fluidization. As shown, as the torsion angle was increased, the fluidization capacity continued to increase. When the torsion angle was small, the internal blades hindered the overall circulation of the LiF particles inside the bed, so they easily formed a dead zone in the upper portion of the bed. As the blade torsion angle was increased, the transverse component of the gas on the blade assisted with particle stirring and secondary gas distribution, while the longitudinal component of the gas played the role of crushing the particle aggregates, both of which improved the fluidization characteristics of the fluidized bed. When the blade angle was changed from 55° to 60°, the fluidization ability increased by the largest margin, which was the optimum operational performance of the internal blade. If the angle was increased to 65°, the fluidization ability improved, but this increase was significantly less and the channel flow and the slug section increased slightly. Therefore, the optimum angle for the internal blade was concluded to be 60°.

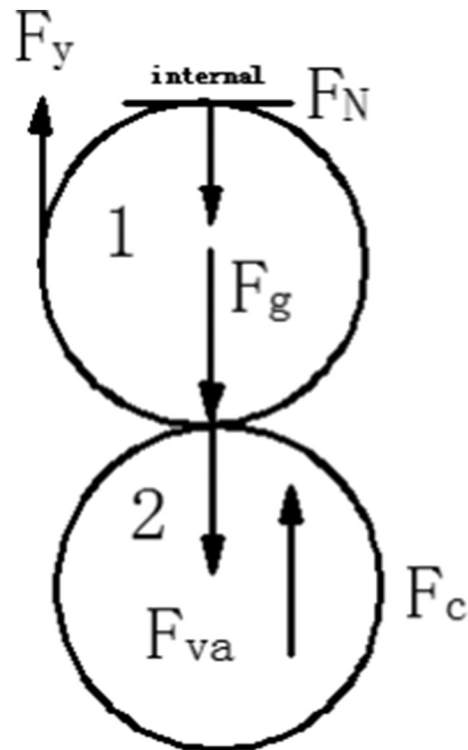


Fig. 16. The force model of agglomeration.

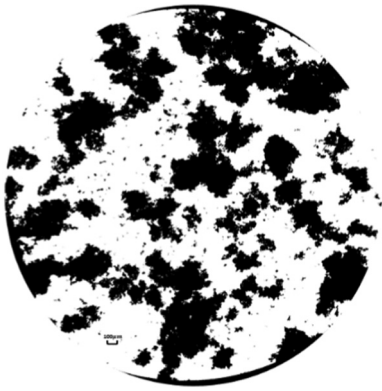


Fig. 17. Microscopic image of agglomeration.

### 3.4. Effect of the internal blade on the fluidization of LiF

Fig. 14 shows the fluidization ability curve for the various types of internal blades. It can be clearly seen from this figure that at fixed blade conditions, the fluidization ability of the internal multi-plate blade was significantly better than the internal single-plate blade. In addition and regardless of being a single plate or a multi-plate blade, the three internal blades provided the best fluidization. A small number of blades will reduce the transverse area that affects the channel flow, while an excessive number of blades would approximate a solid horizontal bed component, which would impede vertical movement of the particles. This would reduce the total circulation capacity of the fluidized bed in the longitudinal direction, and cause the formation of secondary aggregates in the upper portion of the bed.

In the blade characterization experiments, the minimum fluidized gas velocity for single plates with 2, 3 and 4 blades was 0.142 m/s, 0.135 m/s, and 0.155 m/s. The minimum fluidized gas velocity for multiple plates with 2, 3 and 4 blades was 0.135 m/s, 0.125 m/s, and 0.13 m/s. Interestingly, although the minimum gas velocity was the same at 0.135 m/s, the fluidization abilities of the single-plate 3-blade and multi-plate 2-blade were quite different. This was because under the identical fluidization conditions, the multi-plate configuration increased the fluidization in the middle area of the blade, which further established a uniform distribution of the bed pressure drop, thereby reducing the probability of gas channeling. At this time, the expansion rate of the multi-plate bed was also higher than the single plate bed, so relying on the either the minimum fluidization velocity or bed expansion rate criteria to determine quality of bed fluidization will not accurately explain the differences between the single and multi-plate fluidization qualities. However, combining these two parameters with the

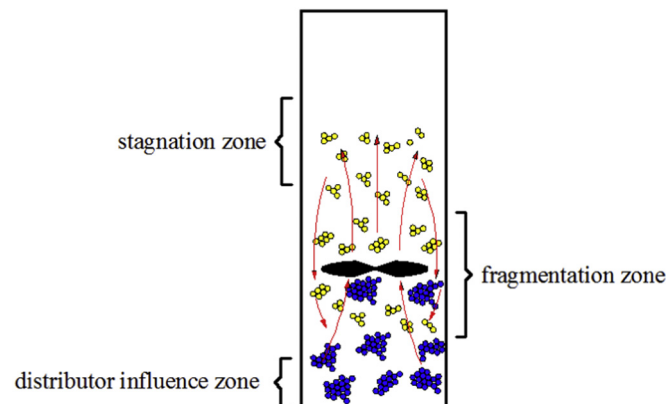


Fig. 18. Effect of balde internal on the LiF agglomerate.

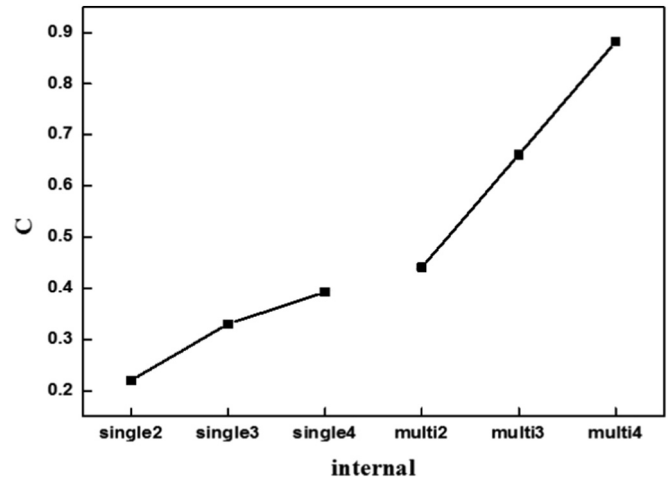


Fig. 19. Collision probability of different blade internals.

dimensionless fluidization ability can correctly establish the real quality of fluidization of a bed.

## 4. Theoretical analysis, results and discussion

Channel flow occurs easily in C-type particle fluidization beds. When internal blades are added to the bed, a pressure drop redistribution at the distributor plate was achieved, together with the disruption of particle aggregates. The mechanism of agglomeration of viscous particles is shown in Fig. 15. As a result of the fluid drag force and collisions between particles, a single particle or agglomerates of viscous particles initial adhere together to form chains of particles of different lengths. These particle chains are then connected and wound together over time to form a dendritic aggregate of particles and clusters of these dendritic particles then form into aggregates of the dendritic particles. Fine particles adhere to the surface of the clusters to form new chains of particles. Meanwhile, some chains on the surface of the cluster break off and are carried away by the air stream in the bed. The particle chain is constantly recombined and the clusters gradually grow. When particle adhesion and desorption on the surface of the cluster attain a dynamic balance, the cluster becomes stable and the size of the cluster is constant. Fluidization of the bed is achieved with a larger cluster. When internal blades are added to the bed, large aggregates collide with blades as a result of flowing gas, producing particle fragmentation and fluidization of smaller aggregates.

Based on this analysis of the mechanism of agglomerate formation, the vertical component of the force of internal blade was used to modify

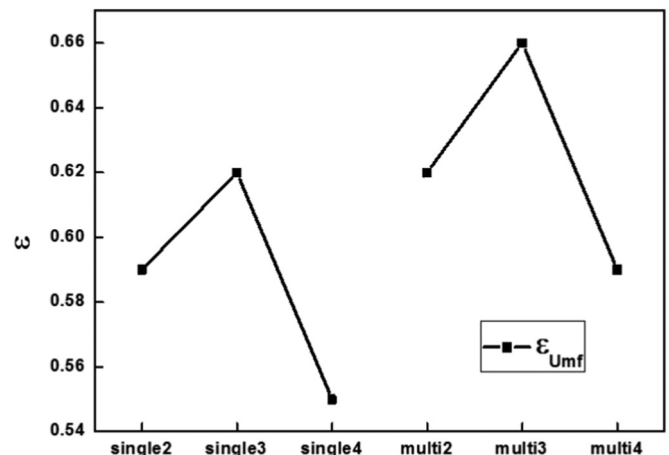


Fig. 20. Expansion rates of different blade internals at the initial fluidization.

**Table 1**

Technical description of the pilot fluidized bed and operating variables.

Parameter	Value
Column height	2000 mm
Column internal diameter	200 mm
Range of rotor flowmeter	0–15 m <sup>3</sup> .h <sup>-1</sup>
Prosity of distribution plates	1.5%
Air flow rate	0–15 m <sup>3</sup> .h <sup>-1</sup>

the original Zhou-Li force balance model [21], from which the particle agglomeration diameter was estimated. Assuming that the probability of collisions between two agglomerates is the highest in the agglomerate fluidized bed, the modified Zhou-Li force balance model is mainly concerned with the collision between two agglomerates.

When the internal blade is added, the force on the agglomerate marked as #1 in this Fig. 16 was analyzed using the Zhou-Li model at the moment of the collision between the blade and the agglomerate [22–25]. As shown in Fig. 16, agglomerate #1 is simultaneously subjected to five forces in the vertical direction, which are the drag force  $F_Y$  of fluid on agglomerate #1, the collision force  $F_C$  of agglomerate #2 on agglomerate #1, the cohesive force  $F_{va}$  of agglomerate #2 on agglomerate #1, the difference between the gravitation force and the buoyancy of agglomerate #1 (apparent gravity) and the vertical force component  $F_N$  of the blade component on the agglomerates. If the upward direction is positive, the resultant force  $y$  of the vertical direction of the agglomerate 1 can be expressed by:

$$y = F_Y + F_C - F_{va} - F_g - F_N \quad (2)$$

when  $y > 0$ , agglomerate #1 may be crushed or it may accelerate upwards; when  $y < 0$ , agglomerate #1 may aggregate with agglomerate #2 or it may generate a downward acceleration, or be crushed. When  $y = 0$ , agglomerate #1 is neither crushed nor aggregated with agglomerate #2, and the whole system is in dynamic equilibrium. Assuming that under ideal conditions, without considering the air resistance, cluster #1 will move vertically upward from the bottom of the bed at the initial velocity of the apparent gas velocity, and according to the law of impulse, the vertical force acting on the cluster when it contacts the internal blade will be:

$$F_N = \frac{\pi}{12} \rho_a U_g d_a^3 \quad (3)$$

According to the Derjaguin approximation theory and Israelachvili's theory of the force between molecules and surfaces, van der Waals force between two agglomerates was expressed as:

$$F_{va} \approx \frac{H_a}{12\delta^2} \frac{d_{a1} d_{a2}}{d_{a1} + d_{a2}} \quad (4)$$

where  $H_a$  is the Hamaker constant,  $d_{a1}$  and  $d_{a2}$  the mean particle diameter of clusters 1 and 2, respectively, and  $\delta$  the distance between two departing particles. Assuming that the fluidized bed was homogeneous and the agglomerate size also homogeneous, Eq. (4) was simplified to

$$F_{va} \approx \frac{H_a d_{a1}}{24\delta^2} \quad (5)$$

$H_a$  was then calculated by the following equation:

$$H_a = 0.75BT \left( \frac{\varepsilon_1 - \varepsilon_0}{\varepsilon_1 + \varepsilon_0} \right)^2 + \frac{3h\nu_e}{16\sqrt{2}} \frac{(N_1^2 - n_0^2)^2}{(N_1^2 + n_0^2)^{3/2}} \quad (6)$$

where  $B$  is the Boltzmann constant ( $B = 1.381 \times 10^{-23}$  J/K),  $T$  the absolute temperature,  $h$  Planck's constant ( $h = 6.626 \times 10^{-34}$  J·s),  $\nu_e$  the

ultraviolet (UV) adsorption frequency, typically at  $\sim 3.0 \times 10^{15}$  s<sup>-1</sup>, and  $\varepsilon_0$  and  $n_0$  the dielectric constant and refractive index, respectively, ( $\varepsilon_0 = 1$ ,  $n_0 = 1$ ). Assuming two agglomerates collide in one direction, the agglomerates were considered to be elastic bodies and the relative collision velocity between the two agglomerates represented by  $V$ . Using Timoshenko and Goodier's theory of elasticity, the displacement of maximum compression  $a$  was.

$$\alpha = \left( \frac{5}{4} \frac{V^2}{n_1 n_2} \right)^{2/5} \quad (7)$$

when  $n_1$  and  $n_2$  are given respectively:

$$n_1 = \sqrt{\frac{8}{9\pi^2(k_1 + k_2)^2}} \sqrt{\frac{d_{a1} d_{a2}}{d_{a1} + d_{a2}}} \quad (8)$$

$$n_2 = \frac{m_1 + m_2}{m_1 m_2} \quad (9)$$

where  $m_1$  and  $m_2$  are the mass of agglomerates 1 and 2, respectively. Because the properties of these agglomerates were the same,  $k_1 = k_2 = k$ , which yields:

$$\alpha = \left[ \frac{5V^2 \pi^2 k \rho_a d_{a1}^3 d_{a2}^3}{8(d_{a1}^3 + d_{a2}^3)} \sqrt{\frac{d_{a1} + d_{a2}}{2d_{a1} d_{a2}}} \right]^{2/5} \quad (10)$$

when  $k$  was a function of Poisson's ratio  $\nu$  and modulus of elasticity  $E$ :

$$k = \frac{1 - \nu^2}{\pi E} \quad (11)$$

Therefore, the collision force between agglomerates 1 and 2 was:

$$F_C = 0.2516 \left[ \frac{\pi V^6 \rho_a^3}{k^2} \left( \frac{d_{a1}^{10}}{8} \right) \right]^{1/5} \quad (12)$$

Because the movement of particles or agglomerates in a fluidized bed involved turbulent flow, the formulation of a kinetic or drag force might be given by Eq. (10):

$$F_Y = 0.055 \pi \rho_f d_{a1}^2 U_g^2 \varepsilon^{-4.8} \quad (13)$$

where  $\rho$  is the fluid density,  $u$  the superficial gas velocity, and  $\varepsilon$  the bed voidage.

For agglomerate 1, the difference between the gravitational force and buoyancy acting on it was:

$$F_g = \frac{\pi}{6} (\rho_a - \rho_f) d_{a1}^3 g \quad (14)$$

If the resultant force in the vertical direction is zero and the diameters of agglomerate #1 and agglomerate #2 are equal to  $d_a$ , the modified force balance equation can be expressed as Eq. (15):

$$\left[ (\rho_a - \rho_f) g + \frac{1}{2} \rho_a U_g \right] d_a^2 - \left[ 0.33 \rho_f U_g^2 \varepsilon^{-4.8} + \frac{0.996}{\pi} \left( \frac{\pi V^8 \rho_a^2}{k^2} \right)^{1/3} \right] d_a + \frac{A}{4\pi z_0^2} = 0 \quad (15)$$

**Table 2**  
The agglomeration size of LiF with blade internal.

blade number	Single internal			Multi internal		
	$d_{ac1}(\mu\text{m})$	$d_{ac2}(\mu\text{m})$	$d_{am}(\mu\text{m})$	$d_{ac1}(\mu\text{m})$	$d_{ac2}(\mu\text{m})$	$d_{am}(\mu\text{m})$
2-blades	679	692	621	635	653	573
3-blades	664	685	613	588	624	536
4-blades	707	721	647	640	661	602

$$(\rho_a - \rho_f)gd_a^2 - \left[ 0.33\rho_f U^2 g \varepsilon^{-4.8} + \frac{0.996}{\pi} \left( \frac{\pi V^8 \rho_a^2}{k^2} \right)^{\frac{1}{3}} \right] d_a + \frac{A}{4\pi z_0^2} = 0 \quad (16)$$

The original Zhou-Li equation is Eq. (16). Table 2 shows a comparison between the calculated values of the agglomerate model equations ( $d_{ac2}$  and  $d_{ac1}$ ) and the experimental values ( $d_{am}$ ). Microscopic image of agglomeration was shown in Fig. 17. As shown,  $d_{ac2}$  was obtained from the original Zhou-Li equation and  $d_{ac1}$  is the correction value for the modified Zhou-Li equation.

It can be seen from the results listed in Table 2 that the calculated values from the modified Zhou-Li equation were better than those obtained from the unmodified Zhou-Li equation, so that the modified equation appeared to offer a better of the size of LiF agglomerates.

Fig. 18 depicts how the blade crushes the LiF agglomerate. It can be seen in this figure that the fluidized bed is divided into three zones which include, the distributor influence zone, the fragmentation zone and the stagnation zone. The gas enters the bed through the distribution plate which drives the particle fluidization. The area affected by the distribution plate is the area where the particle movement is controlled by the action of the gas being emitted by the hole in the distribution plate. The fluidization effect is directly related to the distribution effect of the distribution plate. The fragmentation zone is located between distribution plate and internal blade component, where the agglomerates collide to form fragments after impacting the with blade that are rotated by the gas. The stagnation zone is located above the blade component, where the particles reaggregate to form clusters.

To some extent, the fragmentation of the aggregates can be positively correlated with the collision probability between the aggregates and the blades. The ratio of the projected area of the blades in the vertical direction to the cross-sectional area of the bed is defined as the generalized collision probability  $C$ . The generalized collision probability of various internal blades is shown in Fig. 19. Theoretically, a larger number of blades will produce a greater collision probability between the aggregates and the blades, which will improve the fragmentation of the particulate aggregates. It is easier to fluidize the bed into smaller aggregates with the entrapment of gases. The fluidization quality should be positively correlated to the collision probability  $C$ , but this was not what the experimental results showed.

Fig. 20 shows the expansion rates of the various internal blade combinations at the initiation of bed fluidization. The bed expansion rate directly affects the gas-solid drag and the solid-solid viscous force. To ensure the fluidization of viscous particles, the biggest obstacle is uneven gas distribution and gas short circuiting in the entirety of the bed. The bed

expansion rate is directly related to the gas distribution effect. Higher bed expansion rates will produce smaller cohesive forces between the solids, which will increase the fluidization of the viscous particles.

The addition of blades to the fluidized bed will improve the bed's expansion rate, while the blade itself will hinder the overall circulation of the bed. Therefore, addition of a single blade components to a bed produces a a contradictory relationship, and the extreme value for this contradiction appears in the accompanying figure. The multi blade configuration is used to increase the component influence zone, and the fluidization effect is also significantly better than with the single blade, but the contradictory relationship with this configuration is also present. When a two blade component is used, the particle circulation throughout the entire bed is improved, the bed voidage is largely the same, but the crushing capacity is poor. When 4 the blades are used it was found that too many blades hindered the particle circulation of the fluidized bed and split the bed into two circulation regions. The crushing effecting the bottom region was quite evident, but particle circulation in the upper area of the bed decreased and the particle re-agglomeration occurred. Therefore, the 3 blade configuration takes into account the overall circulation of the bed and the crushing capacity of the fluidized bed and produced the optimum fluidization effect.

## 5. Conclusions

The fluidization quality of LiF particles in a fluidized bed can be improved by the addition of internal mixing blades. The fluidization of the system is significantly affected by the installation height, torsion angle and the number of internal blades. When the installation height was 15 cm, the torsion angle was  $60^\circ$  and three blades were used, the best fluidization results were obtained. It was also found that a multi-blade system was better than a single-plate blade.

The internal blade increased the fracture of particle aggregates, as well as the voidage of the bed. A modified Zhou-Li equation was developed to take into account the vertical force component of the blade on the agglomerates and the modified equation was found to offer a better prediction of the size of the agglomerates after the internal blade was added.

With the increase in the number of blades, the probability of particle collisions increased linearly. In addition, the vertical component of the gas velocity decreased, and too many blades were found to hinder the overall circulation of the fluidized bed, splitting the bed into two parts. In the bottom section of the divided bed good agglomerate fracture was observed, while in the upper section of the bed the particle flow dead zone area increased, and the particles re-agglomerated. Therefore, addition of the 3 blades to the bed simultaneously solves the overall circulation and agglomerate breaking problems of the fluidized bed, offering the best solution to these problems.

## Acknowledgments

The authors appreciate the financial support from National Key R&D Program of China.

## Declaration of Competing interest

None.

## Appendix A. Appendix

The experimental data of LiF with blade internal

$U_{mf}$ , m/s				$\varepsilon$ (bed voidage, $h_0 = 22$ cm)			
Installation height (60°,3-blades)	Torsion angle (15 cm)	Single plate, (15 cm,60°)	Multi plate, (15 cm,60°)	Installation height (60°,3-blades)	Torsion angle (15 cm)	Single plate, (15 cm,60°)	Multi plate, (15 cm,60°)
0.181 (10 cm)	0.172 (50°,3-blades)	0.142 (2-blades)	0.135 (2-blades)	0.34 (10 cm)	0.33 (50°,3-blades)	0.58 (2-blades)	0.61 (2-blades)
0.158 (13 cm)	0.163 (55°,3-blades)	0.135 (3-blades)	0.125 (3-blades)	0.42 (13 cm)	0.35 (55°,3-blades)	0.63 (3-blades)	0.65 (3-blades)
0.133 (15 cm)	0.135 (60°,3-blades)	0.155 (4-blades)	0.130 (4-blades)	0.55 (15 cm)	0.47 (60°,3-blades)	0.55 (4-blades)	0.57 (4-blades)
0.148 (17 cm)	0.133 (65°,3-blades)			0.43 (17 cm)	0.55 (65°,3-blades)		
0.176 (20 cm)				0.32 (20 cm)			

## References

- [1] Z.X. Shu, R.S. Mcmillan, J.J. Murray, Use of chloroethylene carbonate as electrolyte solvent for a graphite anode in a lithium-ion battery[J], *J Electrochem Soc* 43 (7) (1996) 2230–2235.
- [2] H.S. Lee, X.Q. Yang, X. Sun, et al., Synthesis of a new family of fluorinated boronate compounds as anion receptors and studies of their use as additives in lithium battery electrolytes[J], *J Power Sources* 97–98 (2001) 566–569.
- [3] Jaber Shabanian, Jamal Chaouki, Hydrodynamics of a gas–solid fluidized bed with thermally induced interparticle forces, *Chem. Eng. J.* 259 (2015) 135–152.
- [4] Y. Mawatari, Y. Tatemoto, K. Noda, Prediction of minimum fluidization velocity for vibrated fluidized bed, *Power Technol.* 131 (2003) 66–70.
- [5] R.M. Wilhelm, M. Kwauk, Fluidization of solid particles, *Chem. Eng. Prog.* (1948) 201–207.
- [6] R.L. Brown, J.C. Richards, *Principles of Powder Mechanics: Essays on the Packing and Flow of Powders and Bulk Solids*[M], Elsevier, 2013.
- [7] C.M. Chen, L.P. Leu, Hydrodynamics and mass transfer in three-phase magnetic fluidized beds, *Power Technol.* 117 (2001) 198–206.
- [8] T. Zhou, H.Z. Li, K. Shinohara, Agglomerating fluidization of group C particles: major factors of coalescence and breakup of agglomerates, *Adv. Power Technol.* 17 (2) (2006) 159–166.
- [9] H.P. Liu, L.Y. Zhang, Experimental study on the fluidization behaviors of the super-fine particles, *Chem. Eng. J.* 262 (2015) 579–587.
- [10] C.Q. LaMarche, P. Liu, K.M. Kellogg, Fluidized-bed measurements of carefully-characterized, mildly-cohesive (Group A) particles, *Chem. Eng. J.* 310 (2017) 259–271.
- [11] J. Wang, B. Xu, et al., Agglomeration mechanism of nanoparticles by adding coarse fluid catalytic cracking particles[J], *Chem. Eng. Technol.* 39 (18) (2016).
- [12] E. Cano-Pleite, Y. Shimizu, et al., Effect of vertical vibration and particle size on the solids hold-up and mean bubble behavior in a pseudo-2D fluidized bed, *Chem. Eng. J.* 304 (2016) 384–398.
- [13] Q.J. Guo, H. Liu, et al., Influence of sound wave characteristics on fluidization behaviors of ultrafine particles, *Chem. Eng. J.* 119 (2006) 1–9.
- [14] P.J. Jiang, H. Bi, et al., *Fluidization Science and Technology*, Conference Papers, Fourth China-Japan Symp. 1, Science Press, Beijing, China, 1991.
- [15] Q. Liu, Improvement of fluidization quality of cohesive particles by internals [D], *Chin. J. Process Eng.* (2000) Graduate School of Chinese Academy of Sciences.
- [16] Antonio, Jose Manuel, Fluidization of nanoparticles: a simple equation for estimating the size of agglomerates, *Chem. Eng. J.* 140 (2008) 296–304.
- [17] J. Chaouki, C. Chavarie, D. Klvana, et al., Effect of Interparticle forces on the hydrodynamic behavior of fluidized aerogels, *Powder Technol.* 43 (2) (1985) 117–125.
- [18] S. Morooka, K. Kusakabe, A. Kokata, et al., Fluidization state of ultrafine powders, *J. Chem. Eng. Japan* 21 (1988) 41–46.
- [19] D. Gidaspow, *Multiphase Flow and Fluidization*, Academic Press, Inc, 1994.
- [20] T. Zhou, H.Z. Li, Estimation of agglomerate size of cohesive particles during fluidization, *Powder Technol.* 101 (1) (1999) 57–62.
- [21] T. Zhou, H.Z. Li, *Powder Technol.* 101 (1) (1999) 57.
- [22] W.R.A. Goossens, G.L. Dumont, G.L. Spaepen, Fluidization of binary mixtures in the laminar flow region[J], *Chem. Eng. Prog. Symp. Ser.* 67 (116) (1971) 38–45.
- [23] H. Krupp, Particle adhesion, theory and experiment[J], *Adv. Colloid Interface Sci.* 1 (1967) 111.
- [24] M. Horio, Y. Iwadate, The Prediction of Sizes of Agglomerates Formed in Fluidized Beds: Proc. of the 5th World Congress of Chem. Engineering, 2nd Intl. Particle Technology Forum[C], San Diego: American Institute of Chemical Engineers, 1996 722–731.
- [25] D. Geldart, The effect of particle size and size distribution on the behaviour of gas-fluidised beds[J], *Powder Technol.* 6 (4) (1972) 201–215.